ACS APPLIED MATERIALS & INTERFACES

Research Article

www.acsami.org

Highly Resolved Nanostructured PEDOT on Large Areas by Nanosphere Lithography and Electrodeposition

Van-Quynh Nguyen, Delphine Schaming, Pascal Martin, and Jean-Christophe Lacroix*

Université Paris Diderot, Sorbonne Paris Cité, ITODYS, UMR 7086 CNRS, 15 rue Jean-Antoine de Baïf, 75205 Paris Cedex 13, France

Supporting Information

ABSTRACT: Poly(ethylenedioxythiophene) (PEDOT) films were electrodeposited galvanostatically from an EDOT/sodium dodecyl sulfate solution in water, through a carboxylated polystyrene template monolayer self-assembled on ITO, after which the template was dissolved away in tetrahydrofuran. Analysis of the films by scanning electron microscopy and atomic force microscopy reveals large-area PEDOT honeycomb structures. The morphology of these structures was varied electrochemically, as the effective thickness and, surprisingly, the shape of the honeycomb arrangement depend on the polymerization time. Using nanospheres of 1 μm diameter and charge densities between 12 and 30 mC cm^{-2} for electrodeposition generates PEDOT hexagons with very thin rectilinear walls 30−35 nm-thick and 800 nm-long, whereas at higher charge densities, circular bowls are created with 60 nm walls separating adjacent bowls; triangular areas as small as 0.02 μm^2 develop at the intersection of three nanospheres. These morphologies are specific to the use of carboxylated PS spheres and a water-based solution with a surfactant in the galvanostatic electrodeposition mode. Using smaller nanospheres, i.e. 500 nm in diameter, makes it possible to reach PEDOT hexagons with rectilinear walls as small as 11−17 nm-thick and 300 nm-long; circular bowls with 25−35 nm walls separating adjacent bowls and triangular areas as small as 0.003 μm^2 can also be generated. The wettabilities of the surfaces depend markedly on the pore depth of the PEDOT nanostructure, with contact angles going from 82° to 130° with increasing pore size. Finally these nanostructured PEDOT electrodes were used in Grätzel-type dye-sensitized solar cells (DSSCs) as Pt-free counter-electrodes, with an increase in the yield from 7.0 (bulk PEDOT) to 8.1%.

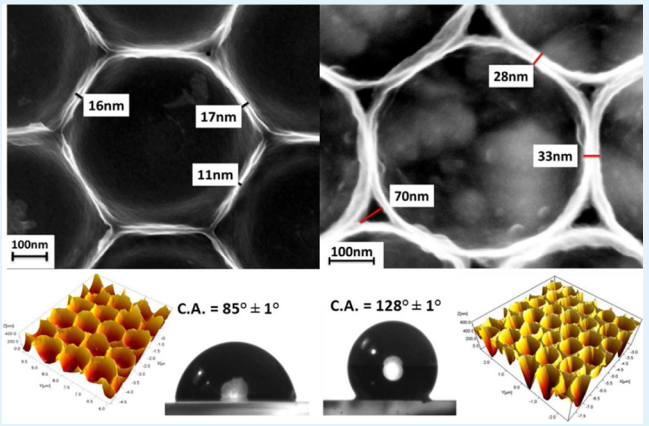

KEYWORDS: *PEDOT, nanostructuration, nanosphere lithography, DSSC, conducting polymers, wettability*

INTRODUCTION

Conducting polymers (CPs) have received much attention over the last 30 years because of their potential applications as molecular[1−5] plastic electronic[6,7] and optoelectronic devices,[8,9] biosensors,[10,11] anticorrosion coatings,[12−15] and smart surfaces.[16−18] They are also proposed as solid-state redox shuttles[19] and counter-electrodes[20−25] in Grätzel type solar cells. Conducting polymers are typically synthesized by chemical or electrochemical oxidative polymerization. Significant advantages of electropolymerization are the low cost, the short fabrication time, the ease of preparation, and the possibility of controlling both the growth rate and the amount of polymer deposited.[26]

Nanostructuring plays an important role in improving the performance or in extending the functionalities of many materials, devices, or products.[27−32] Electron beam lithography is the conventional method for generating highly resolved nanostructured materials with emphasis on the control of morphology, shape, and size. Nevertheless, this technique is expensive and cannot be used for large-area nanopatterning, which hinders its use for mass production. Photolithography is, on the contrary, widely used in industry but reaches a size limit, as the resolution cannot be less than the wavelength of the light used. Hence, research has tended to focus on the development of new routes for fabricating nanostructured materials cheaply, with high resolution and, for some applications (smart surfaces, photovoltaics), on large areas. Spin coating is one of these routes, as some recent works have shown that PEDOT nanowire films can be easily prepared using commercially available PEDOT:PSS solution, followed by a simple post-treatment.[33,34] Nanosphere lithography (NSL) is also a promising method which meets these requirements partially. As a consequence, combining NSL and electropolymerization has been the subject of several studies.

Received: January 14, 2015
Accepted: September 10, 2015
Published: September 10, 2015

DOI: 10.1021/acsami.5b06699
ACS Appl. Mater. Interfaces 2015, 7, 21673−21681

Sumida et al.[35] were the first to report the electrochemical preparation of macroporous polypyrrole films (PPy) using NSL on F-doped SnO_2-coated glasses. Shortly afterward, Bartlett et al.[36] described a general approach for the synthesis of various highly ordered macroporous conducting films of PPy, polyaniline, and polybithiophene and evidenced a "guiding effect" induced by the templates. More recently, micro/nanostructured poly(ethylenedioxythiophene) (PEDOT)[37] and even ultrathin nanostructured organic layers obtained by the reduction of diazonium salts[38−41] have been produced via NSL on glassy carbon, indium−tin oxide (ITO), and noble metals. NSL was used for the electrochemical preparation of nanoporous/inverse opal CP structures with potential biosensing applications.[42−46] It was employed to electrosynthesize macro/mesoporous CPs to generate optoelectronic devices like photonic crystals,[47] organic light-emitting diodes (OLED),[48] and solar cells,[49] as well as photosensitive[50] and smart surfaces with switchable wettability on an ITO-coated glass substrate and various oxidable metals.[51,52]

This work describes the preparation and the use of various large-area honeycomb PEDOT nanostructures on ITO surfaces generated through a monolayer of carboxylated polystyrene (PS) nanospheres used as a template for electropolymerization of EDOT from an aqueous solution containing sodium dodecyl sulfate (SDS). We wish to investigate how the carboxylated PS spheres and/or the use of an aqueous solution containing surfactants affect the morphologies of the PEDOT structures in terms of effective thickness, the shape of the honeycomb arrangement, and the size of the walls growing within the interstitial voids of the PS assemblies. We also consider the impact of such nanostructuration in two fields of PEDOT application, i.e. smart surfaces and dye-sensitized solar cells (DSSCs). Surface wettability has been studied, and nanostructured electrodes were tested in Grätzel-type DSSCs as Pt-free counter-electrodes.

EXPERIMENTAL SECTION

Chemicals and Reagents. 3,4-Ethylenedioxythiophene (EDOT) was purchased from Bayer and distilled before use. Lithium perchlorate ($LiClO_4$) and SDS were used as received without further purification. The monodisperse carboxylate-modified PS spheres have a diameter of 1.02 μm (Sigma-Aldrich, 10 wt % solution in water). All aqueous solutions were freshly prepared with ultrapure water (Milli-Q, 18.2 MΩ cm).

Instrumentation. Electrochemical experiments were performed in a conventional three-electrode configuration (CH Instruments, CHI 440A). The working electrode was ITO modified by a PS nanosphere template; a saturated calomel electrode (SCE) and a large-area platinum mesh were used as reference and counter-electrodes, respectively.

Surface morphology was characterized by scanning electron microscopy (SEM, Zeiss supra 40). PEDOT nanostructure topography and thickness were observed by atomic force microscopy (AFM) in the tapping mode with silicon AFM probes (Tap300-G, stiffness constant k = 40 N·m^{-1} and resonance frequency 300 kHz). Surface wettability was measured by a Digidrop contact angle meter. Measured contact angles are advancing contact angles.

Colloidal Template Preparation and PEDOT Electrodeposition. The various steps in the fabrication of nanostructured films are shown in Figure 1. The conductive substrates (ITO or FTO (Fluor Tin Oxide)) were first pretreated, by sonication for 1 h in a cleaning solution ($H_2O/NH_4OH/H_2O_2$ (5:1:1 by volume)), in order to increase the hydrophilic properties of their surfaces. Next, the PS spheres were deposited by drop coating, the volume and concentration of the suspension being optimized to allow the formation of a dense monolayer after evaporation of the water. The PS spheres were diluted

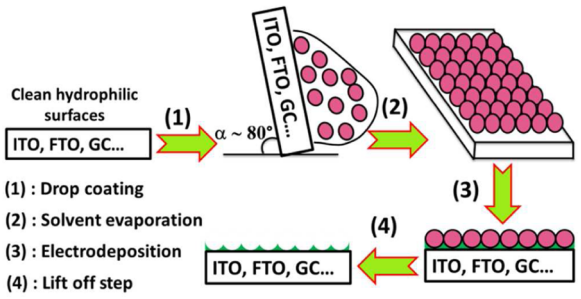

Figure 1. Scheme for generating PEDOT nanostructure using electrochemically assisted NSL.

to 0.5 wt % in water, and a 10 μL droplet was placed on the flat hydrophilic electrode surface. The electrodes were tilted at about 80° to the horizontal, and the solvent was allowed to evaporate at room temperature for 1 h. This procedure can be used to obtain large-area (1 cm^2) nanosphere monolayers; the electrodes for electrochemical experiments were 0.2−0.25 cm^2 in the area, and those for DSSC counter-electrodes were 0.5 cm^2. Other methods, such as spin coating, dip coating, and Langmuir−Blodgett coating, have been used to fabricate nanosphere templates but were less easy to optimize in the present case.

PEDOT was deposited in the interstitial voids of the nanosphere template by polymerizing EDOT from an aqueous solution containing 0.02 M EDOT, 0.1 M SDS, and 0.1 M $LiClO_4$. Electropolymerization was performed galvanostatically with an applied current density between 0.5 and 1 mA cm^{-2}, and the deposition time was calculated to control the thickness of the polymer film. Finally, the modified electrode was immersed in THF for 24 h to dissolve away the PS and reveal the nanostructured PEDOT.

Preparation and Study of Dye-Sensitized Solar Cells. Solar cells were built according to the general procedure[24] using the ruthenium Z907 complex as dye and an electrolytic solution containing 0.1 M I_2, 0.1 M LiI, 0.6 M tetra-*n*-butylammonium iodide, and 0.5 M 4-*tert*-butylpyridine in acetonitrile. They were studied under 1 sun illumination (AM 1.5; 100 mW·cm^{-2}) using a solar simulator (Newport) calibrated with a standard silicon cell (Oriel). A potentiostat/galvanostat (CH Instruments 660C) was used to record J−V curves.

RESULTS AND DISCUSSION

Figure 2a shows an example of a PS monolayer deposited on ITO by drop coating. Although some defects or narrow empty spaces are seen between each domain, 0.5 cm^2 electrodes covered with such monolayers were routinely obtained. Next PEDOT was generated from EDOT in the presence of SDS, with $LiClO_4$ as supporting electrolyte, in water at constant current density. In this medium EDOT is oxidized at low potential, and PEDOT is obtained with "guiding effects" associated with the use of surfactant molecules.[53] It has, therefore, been used a great deal to produce nanostructured PEDOT objects such as nanowires with high conductivity.[54−57]

The inset in Figure 2b shows that the electrode potential is stable at 0.9 V during the entire deposition process. This low value, compared to that in acetonitrile, indicates that EDOT radical-cations are stabilized by strong interactions with SDS anions[53] and possibly with the carboxylate groups on the PS spheres. This methodology has a number of advantages, among which is the ease of controlling the film thickness by changing the charge used for deposition. If the deposition yield is assumed to be 100%, the amount of polymer deposited n, expressed as the number of EDOT units, is given by $n = Q/n_eF$ where $Q = I{\cdot}t$ is the charge used for polymerization; n_e is the effective number of electrons associated with PEDOT growth

DOI: 10.1021/acsami.5b06699
ACS Appl. Mater. Interfaces 2015, 7, 21673−21681

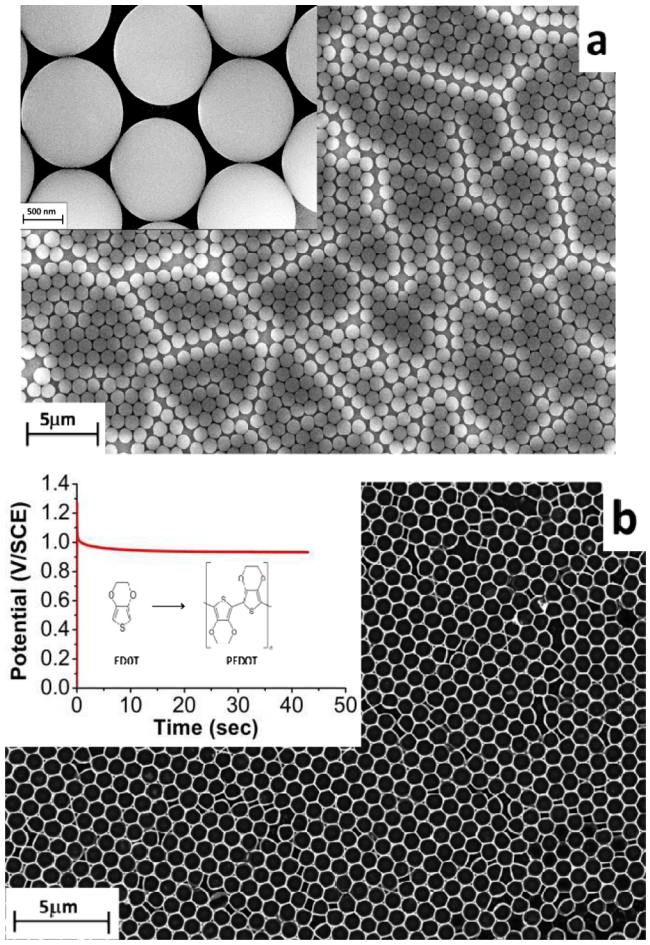

Figure 2. a) Monolayer of PS spheres on ITO. Inset: zoom on the organized PS spheres on ITO; b) Honeycomb structure obtained after depositing PEDOT and dissolving the PS spheres. Inset: galvanostatic deposition curve in 0.02 M EDOT, 0.1 M SDS, and 0.1 M $LiClO_4$ in water at constant 1 mA cm^{-2} current density.

per EDOT monomer (taken as 2.2, since PEDOT is generated in its oxidized state), F is the Faraday constant, and I is the constant current used. The polymer occupies a volume V equal to $S{\cdot}e$ where S is the electrode area, and e is the film thickness. This volume is also equal to $n{\cdot}M/\rho$ where M is the molecular weight of EDOT plus 0.2 times that of the counterion, and ρ is the polymer density (reported to be 1.5).[58] The film thickness is expressed by

$$e = \frac{(M_{\mathrm{EDOT}} + 0.2M_{\mathrm{dodecyl\ sulfate}})}{2.2F\rho}\frac{Q}{S} \qquad (1)$$

which indicates that, on a bare electrode, a charge density of 10 mC cm^{-2} generates a uniform film about 65 nm-thick. When deposition occurs at constant current on a planar surface, the thickness of the film deposited can be easily controlled by changing the deposition time.

In the present case, the electrode surface is modified by nanospheres, between which the polymer grows, and honeycomb PEDOT structures with pores corresponding to the sphere diameter are generated. As a consequence, the pore depth in the nanostructured PEDOT is different from the thickness on a bare planar electrode and does not correlate linearly with the charge density used. Nevertheless, the volume of the free space between the nanospheres can be determined

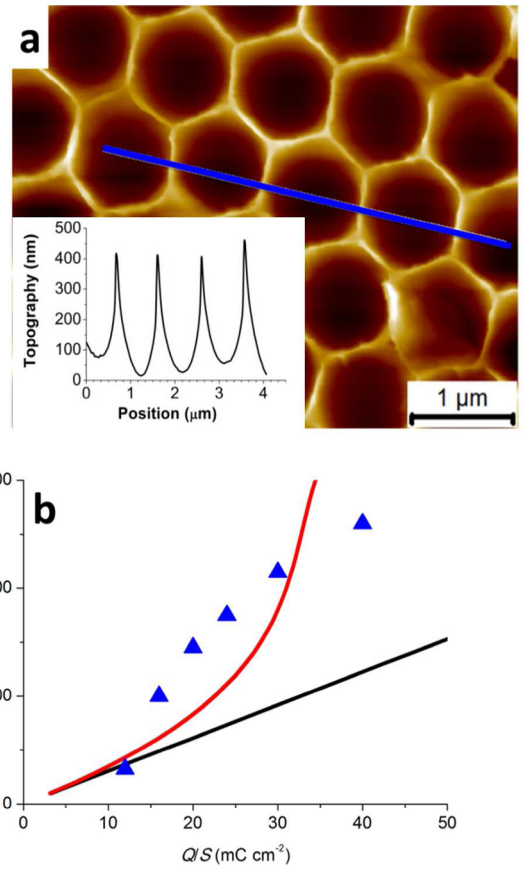

Figure 3. a) AFM image of a nanostructured PEDOT film generated using 25 mC cm^{-2} charge density. Inset: topographic profile of the surface. b) Measured (blue triangles) and theoretical (red curve) pore depths and estimated thickness of film deposited on a bare electrode (black curve) as a function of the charge density.

and is given by eq 2, and, consequently, the theoretical charge required to obtain a given pore depth, e, can be expressed as eq 3 (see Figure S1)

$$V_{\mathrm{free}} = NV_{\mathrm{cavity}} = \frac{S}{\sqrt{3}R^2}\left(\sqrt{3}R^2e - \frac{\pi}{2}Re^2 + \frac{\pi}{6}e^3\right) \qquad (2)$$

$$\frac{Q}{S} = \frac{2.2F\rho e}{M_{\mathrm{EDOT}} + 0.2M_{\mathrm{dodecyl\ sulfate}}}\left(1 - \frac{\pi}{2\sqrt{3}}\frac{e}{R} + \frac{\pi}{6\sqrt{3}}\frac{e^2}{R^2}\right) \qquad (3)$$

with R being the sphere radius (510 nm).

In order to investigate the correlation between the thickness and the charge density, the pore depth of several nanostructured PEDOT films was measured by AFM, and the values compared with the thickness were estimated on the basis of two different assumptions (i) that PEDOT growth is performed on a bare electrode (eq 1) and (ii) that all the cavities between the nanospheres are filled (eq 3). Figure 3a shows an AFM measurement for a charge density of 24 mC cm^{-2}. Pores about 350 nm-deep are obtained (inset). As expected, this much exceeds the 150 nm estimated for a uniform film on a bare electrode (eq 1). However, it also exceeds the theoretical value (around 200 nm, eq 3). Figure S2 shows other AFM images for charge densities of 16 and 40 mC cm^{-2} and average pore depths of 200 and 550 nm, respectively.

Figure 3b displays the average pore depth (blue triangles) as a function of the charge density used for electropolymerization.

DOI: 10.1021/acsami.5b06699
ACS Appl. Mater. Interfaces 2015, 7, 21673−21681

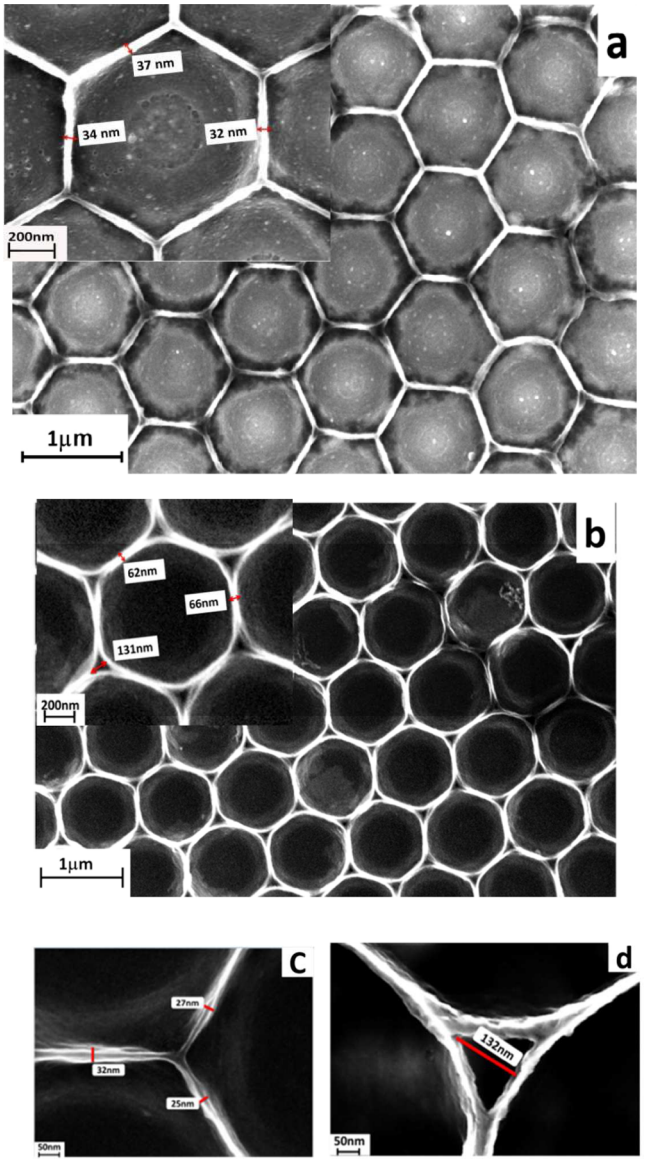

Figure 4. SEM images of nanostructured PEDOT after removal of PS: a) Hexagonal morphology (charge density around 20 mC cm^{-2}); b) Round morphology (40 mC cm^{-2}). c) Zoom showing highly resolved PEDOT nanowires obtained when hexagonal morphologies are generated d) Zoom showing triangular voids between highly resolved PEDOT nanowires obtained when round morphologies are generated.

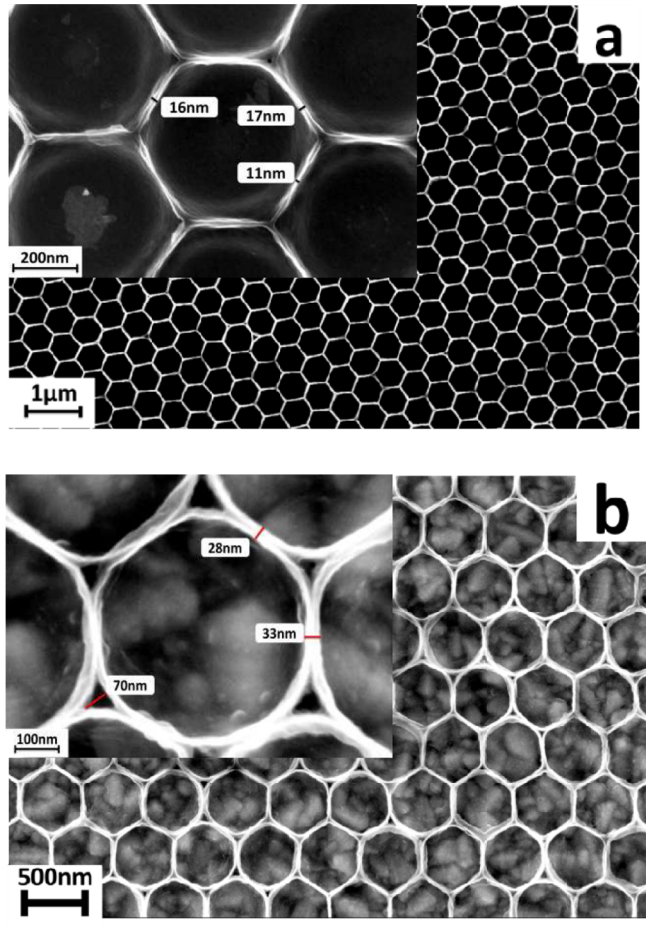

Figure 5. SEM images of nanostructured PEDOT substrates generated using 500 nm diameter PS beads: a) hexagonal morphology (charge density around 11 mC cm^{-2}); b) round morphology (15 mC cm^{-2}).

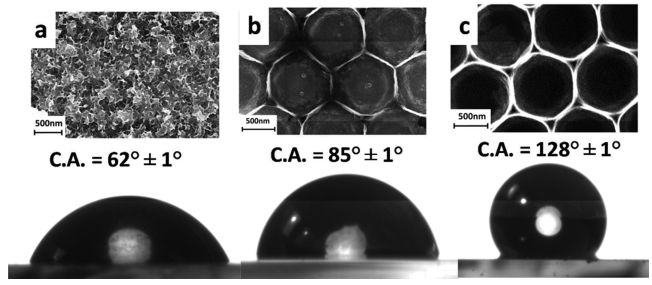

Figure 6. Wettability of surface modified by conducting polymer: a) bulk PEDOT film; b) hexagonal-shaped PEDOT honeycomb; c) bowl-shaped PEDOT honeycomb.

It also shows the estimated thickness (black line) of a PEDOT film generated on a bare electrode, given by eq 1, and the theoretical pore depth (red line), given by eq 3. Two regimes are observed, and the overall behavior is not linear. When the charge density is below 12 mC cm^{-2}, the average pore depth is close to that estimated from eq 3 and also close to the thickness estimated for a bare electrode, as given by eq 1. Indeed, growth is not strongly affected by the PS spheres, as the voids between two spheres remain large enough for PEDOT growth to be like that on a bare electrode. When the charge density is between 12 and 20 mC cm^{-2}, the average pore depth increases with a much sharper slope, going from 80 nm to almost 300 nm, i.e. a third of the PS sphere diameter. Consequently, the measured pore depths are higher than the theoretical values. Finally the growth rate levels off when the charge density is above 25−30 mC cm^{-2} and the pore depth reaches the radius of the PS sphere. For such high charge densities, the pore depths are lower than the theoretical values. Note also that the thickness profile (Figure S2) of the samples shows one maximum located in the middle of a line joining the centers of two spheres when the pores are less than 400 nm deep (see Figure S2a), whereas two maxima are observed when the pore depths are higher than the PS nanosphere radius (see Figure S2b).

These observations have to be correlated with a marked variation of the shape and morphology of the pores with the charge density, as seen in the AFM (Figures 3, S2, and S3) and SEM images (Figure 4). Indeed, when pore depths are below 400 nm, i.e. charge density between 12 and 30 mC cm^{-2}, the pore walls are linear, and, consequently, each pore is hexagonal

DOI: 10.1021/acsami.5b06699
ACS Appl. Mater. Interfaces 2015, 7, 21673−21681

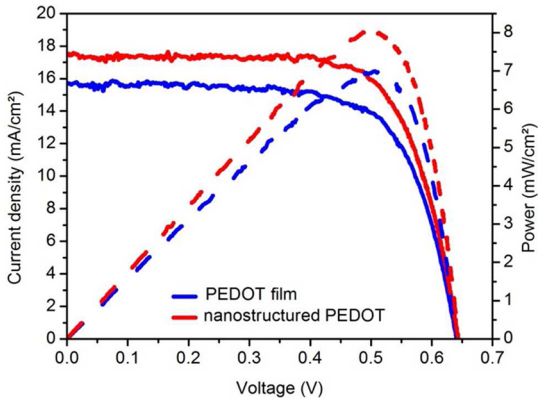

Figure 7. *J*–*V* curves (full lines) and power curves (dashed lines) of DSSCs with bulk (blue curves) and nanostructured (red curves) PEDOT film as counter-electrode.

(Figures 4a and S3a). An exciting result is that the width of one wall is close to 30 nm (see Figure 4a inset and Figure 4c), and its length is close to 800 nm. Note also that these very thin walls are obtained independently of the pore depth. This specific pore shape and wall width cannot be attributed to the confined growth of PEDOT in the voids between the PS spheres, as the space between two adjacent spheres decreases when the amount of PEDOT deposited increases while remaining less than the radius of one nanosphere. This sort of growth should give pores of increasing diameter separated by walls of decreasing width, as observed in other studies.[37,51,52] It cannot be attributed either to PS sphere "guiding effects", as the walls of the pores appear to grow faster halfway between two spheres and not around the PS spheres (see Figure S2b). As a consequence of the void remaining between the nanospheres, the pore depths are higher than the theoretical values, which have been estimated considering that the free space between the nanospheres is completely filled (see Figure 3). These structures are fragile and tend to collapse, revealing in some areas of the surface thin veils of PEDOT which are transparent in SEM. Possible effects occurring postdeposition during the swelling on the PS particles, the dissolution and removal of the template or the drying of the solvent, were not studied.[59] Distortion of the structures has been observed on brittle templates such as oxides and could also be significant here. The effects of strain can lead to distortion and in some cases can tear the structures[60] as observed in Figure 2b. These hexagonal structures are probably due to SDS interaction with the carboxylated nanospheres and EDOT radical-cations, changing the shape of the PS and/or triggering preferential growth perpendicular to the surface.[61] Note that these hexagonal-shaped PEDOT nanostructures can also be obtained at various current densities and using cyclic voltammetry, as long as SDS is present, but not when the SDS concentration is decreased. (See Figure S4 for SEM images of nanostructured PEDOT films produced without SDS.) Even though it is very unlikely that the polymer structure in solution during deposition, when it is swollen by solvent, is the same as that after dissolution of the template and drying, a specific SDS effect is observed.

PEDOT growth is, on the contrary, clearly guided by the carboxylated PS spheres when the pores are deeper than the radius of the nanospheres. Two independent PEDOT skins seem to grow around two adjacent PS spheres, generating circular bowls, as depicted in Figures 4b, S2b, and S3b, with again very thin PEDOT walls separating adjacent bowls. Small concave triangular voids at the intersection of three nanospheres are then created as the result of the formation of round PEDOT objects. In this regime our results are close to those reported by Bartlett et al. for other conducting polymers with dominant growth around the nanospheres.[36] Large nanostructured PEDOT surfaces with very small triangular voids of average side length less than 150 nm and average area less than 0.02 μm^2, as depicted in the inset of Figure 4b and in Figure 4d, can be obtained reproducibly; this underlines the high resolution of the NSL-assisted deposition method used.

We have investigated the feasibility of this procedure on ITO when smaller PS beads are used in order to change the grating, the morphology, and the sizes of the nanostructured PEDOT generated. Figure 5 shows SEM images of a ITO/PS surface, prepared using a 500 nm PS bead template, and modified with 10 mC cm^{-2} (Figure 5a) and 15 mC cm^{-2} (Figure 5b), followed by dissolution of the PS particles. The images show that a PEDOT coating displaying an ordered array of ca. 500 nm equidistant pores with hexagonal morphology, walls 11–17 nm-thick and 300 nm long, can be generated in the former case. When a higher charge density is used for PEDOT growth, PEDOT coating with circular-shaped morphology is again obtained with walls 25–35 nm-thick, and small triangular voids of average side length less than 100 nm and average area less than 0.003 μm^2, as depicted in the inset of Figure 5b. Here again a highly resolved PEDOT structure can be generated on surfaces as large as 1 cm^2, and the use of smaller beads makes it possible to reduce the thickness of the PEDOT walls and the size of the triangular voids created.

These inexpensive nanostructured surfaces obtained here on large areas have interesting wettability and can be used in various applications.

Wettability of the Nanostructured PEDOT Surfaces. Enhanced hydrophobicity with these types of nanostructures has already been demonstrated.[16,18,51,52] In order to investigate these effects the contact angles of a water droplet on the various PEDOT substrates, generated with 1 μm diameter beads, were measured. The PEDOT films are in their oxidized state, and the reported values are averages for 5 different spots on each surface studied. Details can be found in Table S1 along with the pore depth of each sample.

The contact angle on an ITO electrode covered by bulk PEDOT, generated galvanostatically from EDOT in the presence of SDS and $LiClO_4$ in water at constant current density, is 62° (Figure 6a). For the thinnest hexagonal-shaped

Table 1. Photovoltaic Parameters of DSSCs with Bulk and Nanostructured PEDOT Film As Counter-Electrode

	bulk PEDOT film	hexagonal structure 100 nm	hexagonal structure 200 nm	hexagonal structure 300 nm	round structure 500 nm
J_{SC} (mA·cm^{-2})	15.8 ± 0.3	16.7 ± 0.2	17.5 ± 0.1	16.5 ± 0.2	16.1 ± 0.2
V_{OC} (V)	0.64 ± 0.01	0.65 ± 0.02	0.64 ± 0.01	0.64 ± 0.02	0.65 ± 0.01
FF	0.69 ± 0.01	0.73 ± 0.01	0.72 ± 0.01	0.72 ± 0.01	0.73 ± 0.01
η (%)	7.0 ± 0.3	7.9 ± 0.2	8.1 ± 0.1	7.6 ± 0.2	7.6 ± 0.2

DOI: 10.1021/acsami.5b06699
ACS Appl. Mater. Interfaces 2015, 7, 21673–21681

PEDOT nanostructured film it is 85° (Figure 6b). Increasing the pore depth increases the contact angle, with hexagonal PEDOT reaching 125° for a depth of 400 nm, whereas bowl-shaped PEDOT with a pore depth of 550 nm gives a contact angle close to 130° (Figure 6c).

As contact angles increase by increasing the roughness of the PEDOT surface, the systems are governed by the Cassie–Baxter equations.[62] In this regime, air is trapped underneath the droplet. The presence of air effectively lowers the average surface energy[63] and yields hydrophobic apparent contact angles on intrinsically hydrophilic materials ($\theta < 90°$). The apparent contact angle for a Baxter–Cassie state θ_{CB} is given by

$$\cos \theta_{CB} = \varphi_s \cos \theta - (1 - \varphi_s) \quad (4)$$

with φ_s being the fraction of the droplet that is in contact with the PEDOT, and $(1-\varphi_s)$ being the fraction of the droplet in contact with air. Assuming that θ is that of bulk PEDOT, i.e. 62° and θ_{CB} varying from 85° to 130°, we can calculate that φ_s varies from 0.75 for the thinnest hexagonal structure (pore depth 65 nm) to 0.3 for the thickest hexagonal structure (pore depth 440 nm) and reaches 0.25 for bowl-shaped PEDOT with a pore depth of 550 nm. Such values are compatible with the SEM images of the various structures. Similar contact angle variation with thickness has been reported for gold,[64] but, to the best of our knowledge, it has not yet been reported for nanostructured conducting polymers.

Several attempts were performed to increase the contact angle above 130° and to reach superhydrophobic surfaces, but none of them succeeded.[16,65] Indeed, incorporation in bulk PEDOT hydrophobic ions such as diisopropylsalicylate[17] proved to be possible and increased the contact angle of the bulk PEDOT to values close to 90°. However, growing nanostructured PEDOT through 1 μm diameter beads with this ion in the electrolyte did not give the same guiding effect and similar highly resolved PEDOT films. As a consequence φ_s did not reach 0.25, and the apparent contact angle remained close to 130°. Further work is in progress to achieve superhydrophobic behavior.

Overall, large-area PEDOT surfaces, with highly resolved nanostructuration and with controlled contact angle are, therefore, easily obtained by NSL-assisted electrodeposition.

Application As Counter-Electrodes for Enhanced Efficiency in Solar Cells. Conducting polymers play an important role in the field of photovoltaics, particularly in the conception of dye-sensitized solar cells (DSSCs). Grätzel developed solar cells two decades ago, using platinum as the counter-electrode to regenerate the redox mediator in the electrolyte, thanks to its high catalytic activity toward I_3^- reduction.[66] As platinum is a very expensive metal, the use of counter-electrodes of other, cheaper, and more abundant materials is required. A decade ago, PEDOT was reported as the counter-electrode for Pt-free DSSCs,[67] and such PEDOT-based counter-electrodes are now widely used thanks to the good conductivity and electrocatalytic properties for I_3^- reduction.[68] High PEDOT conductivity improves DSSC efficiency,[22,24,25] and nanopatterned structures are much more conductive than uniform films.[69] Moreover, nanostructured materials have higher active catalyst surface areas. Thus, nanostructured PEDOT should be valuable as the counter-electrode in DSSCs. This effect has already been investigated, and high efficiency was observed,[70,25] while a recent study[23] demonstrated a favorable effect on the incident-photon conversion efficiency spectra.

In this context, performances of the nanostructured PEDOT films, generated by NSL-assisted electrodeposition, as counter-electrodes for DSSCs were investigated. DSSCs using photoanodes in TiO_2 photosensitized with the ruthenium dye Z907 and an electrolyte containing the I_3^-/I^- redox mediator were elaborated. Counter-electrodes with honeycomb PEDOT films of various thicknesses and shape (hexagonal/round structures) were used and compared with counter-electrodes of classical bulk PEDOT film. The current density–voltage ($J-V$) characteristic curves of the DSSCs were measured under an illumination of 1 sun (100 mW cm^{-2}).

Typical $J-V$ curves and the corresponding power curves are presented in Figure 7. Important photovoltaic parameters such as the short-circuit current density (J_{SC}), the open-circuit voltage (V_{OC}), the fill factor (FF), and the power conversion efficiency (η) are summarized in Table 1. Values reported are averages from 5 cells for the various types of counter-electrode.

DSSCs with nanostructured PEDOT films exhibit higher J_{SC} and FF values than those with bulk PEDOT films, while V_{OC} remains unchanged. As a result, the efficiency η increases from an average value of 7.0 to 8.1%. Table 1 shows also that FF values do not depend on the thickness and the shape of the used nanostructured film, while J_{SC} varies. As a consequence, there is an optimum thickness for nanostructured PEDOT counter electrode, and the best efficiency (8.1%) is reached when hexagonal structures of 200 nm pore depth are used. Using thicker nanostructured PEDOT films do not yield to better yields as the J_{SC} decreases from 17.5 mA·cm^{-2} to 16.5 mA·cm^{-2} and 16.1 mA·cm^{-2} when the PEDOT thickness increases from 200 to 300 nm (hexagonal structure) and to 500 nm (round structure) These results establish that when nanostructured PEDOT film is used as a counter-electrode the DSSC efficiency increases as the result of a more favorable electrical conductivity or electrocatalytic activity. NSL-assisted PEDOT electrodeposition is thus an interesting alternative to spin-coating techniques generally used to fabricate PEDOT counter-electrodes for DSSCs even though spin coating remains an easier approach.

CONCLUSION

Polyethylenedioxythiophene nanostructures were electrochemically generated using NSL from an EDOT/sodium dodecyl sulfate solution in water. Various honeycomb PEDOT structures were easily obtained over large areas. It is found that the morphology of these structures can be electrochemically controlled, as the pore depth of the structures and, surprisingly, the shape of the honeycomb arrangement depend on the charge density used for polymerization. For 1 μm diameter beads and charge densities between 12 and 30 mC cm^{-2} highly resolved hexagons consisting of linked linear PEDOT walls 30 nm-thick and 800 nm-long are generated, whereas for higher charge densities, circular PEDOT bowls are created with very thin PEDOT walls separating adjacent bowls and triangular areas as small as 0.02 μm^2 growing at the intersections of three nanospheres. Similar structures can also be generated with smaller beads (500 nm diameter) and lead to even smaller features (hexagons with rectilinear walls as small as 11–17 nm-thick, circular bowls with 25–35 nm walls, triangular voids 0.003 μm^2 in area). It is clear that the use of carboxylated PS spheres and a water-based solution of SDS in the galvanostatic electrodeposition mode specifically guides EDOT polymerization. The wettabilities of the surfaces strongly depend on the thickness of the PEDOT honeycomb

DOI: 10.1021/acsami.5b06699
ACS Appl. Mater. Interfaces 2015, 7, 21673–21681

structure, with the contact angle increasing from 85° to 130° as the pore depths increase from 65 to 550 nm. Finally, these nanostructured PEDOT electrodes were used in Grätzel-type DSSCs as Pt-free counter-electrodes. The DSSC yield under 1 sun illumination increases from 7 to 8.1% using these cheap nanostructured large-area PEDOT electrodes.

■ ASSOCIATED CONTENT

Supporting Information

The Supporting Information is available free of charge on the ACS Publications website at DOI: 10.1021/acsami.5b06699.

Eq 3 demonstration, Figures S1−S4, and Table S1 (PDF)

■ AUTHOR INFORMATION

Corresponding Author

*E-mail: lacroix@univ-paris-diderot.fr.

Notes

The authors declare no competing financial interest.

■ ACKNOWLEDGMENTS

This work was supported by the CNRS, the University Paris Diderot (Paris, France) and by a Ph.D. grant from the University of Science and Technology of Hanoi. We are particularly grateful to Dr. J. S. Lomas for revising our text and correcting the English.

■ REFERENCES

(1) Joachim, C.; Gimzewski, J. K.; Aviram, A. Electronics Using Hybrid-Molecular and Mono-Molecular Devices. *Nature* **2000**, *408*, 541−548.

(2) Chen, F.; Tao, N. J. Electron Transport in Single Molecules: From Benzene to Graphene. *Acc. Chem. Res.* **2009**, *42*, 429−438.

(3) Mangeney, C.; Lacroix, J.-C.; Chane-Ching, K. I.; Jouini, M.; Villain, F.; Ammar, S.; Jouini, N.; Lacaze, P.-C. Conducting-Polymer Electrochemical Switching as an Easy Means for Control of the Molecular Properties of Grafted Transition Metal Complexes. *Chem. - Eur. J.* **2001**, *7*, 5029−5040.

(4) Martin, P.; Della Rocca, M. L.; Anthore, A.; Lafarge, P.; Lacroix, J.-C. Organic Electrodes Based on Grafted Oligothiophene Units in Ultrathin, Large-Area Molecular Junctions. *J. Am. Chem. Soc.* **2012**, *134*, 154−157.

(5) Janin, M.; Ghilane, J.; Lacroix, J.-C. When Electron Transfer Meets Electron Transport in Redox-Active Molecular Nanojunctions. *J. Am. Chem. Soc.* **2013**, *135*, 2108−2111.

(6) Facchetti, A.; Mushrush, M.; Yoon, M.-H.; Hutchison, G. R.; Ratner, M. A.; Marks, T. J. Building Blocks for n-Type Molecular and Polymeric Electronics. Perfluoroalkyl- versus Alkyl-Functionalized Oligothiophenes (nT; n = 2−6). Systematics of Thin Film Microstructure, Semiconductor Performance, and Modeling of Majority Charge Injection in Field-Effect Transistors. *J. Am. Chem. Soc.* **2004**, *126*, 13859−13874.

(7) Meng, H.; Bendikov, M.; Mitchell, G.; Helgeson, R.; Wudl, F.; Bao, Z.; Siegrist, T.; Kloc, C.; Chen, C. H. Tetramethylpentacene: Remarkable Absence of Steric Effect on Field Effect Mobility. *Adv. Mater.* **2003**, *15*, 1090−1093.

(8) Baba, A.; Tada, K.; Janmanee, R.; Sriwichai, S.; Shinbo, K.; Kato, K.; Kaneko, F.; Phanichphant, S. Controlling Surface Plasmon Optical Transmission with an Electrochemical Switch Using Conducting Polymer Thin Films. *Adv. Funct. Mater.* **2012**, *22*, 4383−4388.

(9) Stockhausen, V.; Martin, P.; Ghilane, J.; Leroux, Y.; Randriamahazaka, H.; Grand, J.; Felidj, N.; Lacroix, J. C. Giant Plasmon Resonance Shift Using Poly(3,4-ethylenedioxythiophene) Electrochemical Switching. *J. Am. Chem. Soc.* **2010**, *132*, 10224−10226.

(10) Descamps, E.; Leïchlé, T.; Corso, B.; Laurent, S.; Mailley, P.; Nicu, L.; Livache, T.; Bergaud, C. Fabrication of Oligonucleotide Chips by Using Parallel Cantilever-Based Electrochemical Deposition in Picoliter Volumes. *Adv. Mater.* **2007**, *19*, 1816−1821.

(11) Reuillard, B.; Le Goff, A.; Cosnier, S. Non-Covalent Double Functionalization of Carbon Nanotubes with a NADH Oxidation Ru(ii)-Based Molecular Catalyst and a NAD-Dependent Glucose Dehydrogenase. *Chem. Commun.* **2014**, *50*, 11731−11734.

(12) Rohwerder, M.; Michalik, A. Conducting Polymers for Corrosion Protection: What Makes the Difference between Failure and Success? *Electrochim. Acta* **2007**, *53*, 1300−1313.

(13) Tallman, D.; Spinks, G.; Dominis, A.; Wallace, G. Electroactive Conducting Polymers for Corrosion Control. *J. Solid State Electrochem.* **2002**, *6*, 73−84.

(14) Fenelon, A. M.; Breslin, C. B. The Electrochemical Synthesis of Polypyrrole at a Copper Electrode: Corrosion Protection Properties. *Electrochim. Acta* **2002**, *47*, 4467−4476.

(15) Petitjean, J.; Aeiyach, S.; Lacroix, J. C.; Lacaze, P. C. Ultra-Fast Electropolymerization of Pyrrole in Aqueous Media on Oxidizable Metals in a One-Step Process. *J. Electroanal. Chem.* **1999**, *478*, 92−100.

(16) Xu, L.; Chen, W.; Mulchandani, A.; Yan, Y. Reversible Conversion of Conducting Polymer Films from Superhydrophobic to Superhydrophilic. *Angew. Chem., Int. Ed.* **2005**, *44*, 6009−6012.

(17) Hermelin, E.; Petitjean, J.; Lacroix, J.-C.; Chane-Ching, K. I.; Tanguy, J.; Lacaze, P.-C. Ultrafast Electrosynthesis of High Hydrophobic Polypyrrole Coatings on a Zinc Electrode: Applications to the Protection against Corrosion. *Chem. Mater.* **2008**, *20*, 4447−4456.

(18) Wang, X.; Berggren, M.; Inganäs, O. Dynamic Control of Surface Energy and Topography of Microstructured Conducting Polymer Films. *Langmuir* **2008**, *24*, 5942−5948.

(19) Yang, L.; Zhang, J.; Shen, Y.; Park, B.-W.; Bi, D.; Häggman, L.; Johansson, E. M. J.; Boschloo, G.; Hagfeldt, A.; Vlachopoulos, N.; Snedden, A.; Kloo, L.; Jarboui, A.; Chams, A.; Perruchot, C.; Jouini, M. New Approach for Preparation of Efficient Solid-State Dye-Sensitized Solar Cells by Photoelectrochemical Polymerization in Aqueous Micellar Solution. *J. Phys. Chem. Lett.* **2013**, *4*, 4026−4031.

(20) Ahmad, S.; Yum, J.-H.; Xianxi, Z.; Gratzel, M.; Butt, H.-J.; Nazeeruddin, M. K. Dye-Sensitized Solar Cells Based on Poly (3,4-Ethylenedioxythiophene) Counter Electrode Derived from Ionic Liquids. *J. Mater. Chem.* **2010**, *20*, 1654−1658.

(21) Tian, H.; Yu, Z.; Hagfeldt, A.; Kloo, L.; Sun, L. Organic Redox Couples and Organic Counter Electrode for Efficient Organic Dye-Sensitized Solar Cells. *J. Am. Chem. Soc.* **2011**, *133*, 9413−9422.

(22) Ellis, H.; Vlachopoulos, N.; Häggman, L.; Perruchot, C.; Jouini, M.; Boschloo, G.; Hagfeldt, A. PEDOT Counter Electrodes for Dye-Sensitized Solar Cells Prepared by Aqueous Micellar Electrodeposition. *Electrochim. Acta* **2013**, *107*, 45−51.

(23) Park, S. H.; Kim, O.-H.; Kang, J. S.; Lee, K. J.; Choi, J.-W.; Cho, Y.-H.; Sung, Y.-E. Poly(3,4-Ethylenedioxythiophene) Inverse Opal Electrode Fabricated from Poly(3,4-Ethylenedioxythiophene):Poly-(Styrene Sulfonate)-Filled Polystyrene Template for Dye-Sensitized Solar Cells. *Electrochim. Acta* **2014**, *137*, 661−667.

(24) Koussi-Daoud, S.; Schaming, D.; Martin, P.; Lacroix, J.-C. Gold Nanoparticles and Poly(3,4-Ethylenedioxythiophene) (PEDOT) Hybrid Films as Counter-Electrodes for Enhanced Efficiency in Dye-Sensitized Solar Cells. *Electrochim. Acta* **2014**, *125*, 601−605.

(25) Lu, C.-Y.; Tsai, C.-H.; Tsai, Y.-T.; Hsu, C.-J.; Chang, C.-H.; Wu, C.-C. Spontaneous Formation of Nanofibrillar and Nanoporous Structures in High-Conductivity Conducting Polymers and Applications for Dye-Sensitized Solar Cells. *Adv. Energy Mater.* **2015**, *5*, 1401738.

(26) *Electropolymerization: Concepts, Materials and Applications*; Cosnier, S., Karyakin, A., Eds.; Wiley-VCH Verlag GmbH & Co. KGaA: 2010; 280 pp.

(27) Li, C.; Bai, H.; Shi, G. Conducting Polymer Nanomaterials: Electrosynthesis and Applications. *Chem. Soc. Rev.* **2009**, *38*, 2397−2409.

DOI: 10.1021/acsami.5b06699
ACS Appl. Mater. Interfaces 2015, 7, 21673−21681

(28) Nishimoto, S.; Bhushan, B. Bioinspired Self-Cleaning Surfaces with Superhydrophobicity, Superoleophobicity, and Superhydrophilicity. *RSC Adv.* **2013**, *3*, 671−690.
(29) Asefa, T.; Duncan, C. T.; Sharma, K. K. Recent Advances in Nanostructured Chemosensors and Biosensors. *Analyst* **2009**, *134*, 1980−1990.
(30) Tian, J.; Zhao, Z.; Kumar, A.; Boughton, R. I.; Liu, H. Recent Progress in Design, Synthesis, and Applications of One-Dimensional TiO_2 Nanostructured Surface Heterostructures: a Review. *Chem. Soc. Rev.* **2014**, *43*, 6920−6937.
(31) Zaera, F. Nanostructured Materials for Applications in Heterogeneous Catalysis. *Chem. Soc. Rev.* **2013**, *42*, 2746−2762.
(32) Guldin, S.; Hüttner, S.; Kolle, M.; Welland, M. E.; Müller-Buschbaum, P.; Friend, R. H.; Steiner, U.; Tétreault, N. Dye-Sensitized Solar Cell Based on a Three-Dimensional Photonic Crystal. *Nano Lett.* **2010**, *10*, 2303−2309.
(33) Xia, Y.; Sun, K.; Ouyang, J. Solution-Processed Metallic Conducting Polymer Films as Transparent Electrode of Optoelectronic Devices. *Adv. Mater.* **2012**, *24*, 2436−3440.
(34) Kim, N.; Kee, S.; Lee, S. H.; Lee, B. H.; Kahng, Y. H.; Jo, Y.-R.; Kim, B.-J.; Lee, K. Highly Conductive PEDOT:PSS Nanofibrils Induced by Solution-Processed Crystallization. *Adv. Mater.* **2014**, *26*, 2268−2272.
(35) Sumida, T.; Wada, Y.; Kitamura, T.; Yanagida, S. Electrochemical Preparation of Macroporous Polypyrrole Films with Regular Arrays of Interconnected Spherical Voids. *Chem. Commun.* **2000**, 1613−1614.
(36) Bartlett, P. N.; Birkin, P. R.; Ghanem, M. A.; Toh, C.-S. Electrochemical Syntheses of Highly Ordered Macroporous Conducting Polymers Grown around Self-Assembled Colloidal Templates. *J. Mater. Chem.* **2001**, *11*, 849−853.
(37) Santos, L.; Martin, P.; Ghilane, J.; Lacaze, P.-C.; Randriamahazaka, H.; Abrantes, L. M.; Lacroix, J.-C. Electrosynthesis of Well-Organized Nanoporous Poly(3,4-Ethylenedioxythiophene) by Nanosphere Lithography. *Electrochem. Commun.* **2010**, *12*, 872−875.
(38) Maldonado, S.; Smith, T. J.; Williams, R. D.; Morin, S.; Barton, E.; Stevenson, K. J. Surface Modification of Indium Tin Oxide via Electrochemical Reduction of Aryldiazonium Cations. *Langmuir* **2006**, *22*, 2884−2891.
(39) Corgier, B. P.; Bélanger, D. Electrochemical Surface Nanopatterning Using Microspheres and Aryldiazonium. *Langmuir* **2010**, *26*, 5991−5997.
(40) Santos, L.; Ghilane, J.; Lacroix, J.-C. Surface Patterning Based on Nanosphere Lithography and Electroreduction of In Situ Generated Diazonium Cation. *Electrochem. Commun.* **2012**, *18*, 20−23.
(41) Cernat, A.; Griveau, S.; Martin, P.; Lacroix, J. C.; Farcau, C.; Sandulescu, R.; Bedioui, F. Electrografted Nanostructured Platforms for Click Chemistry. *Electrochem. Commun.* **2012**, *23*, 141−144.
(42) Li, H.; Wu, N. A Large-Area Nanoscale Gold Hemisphere Pattern as a Nanoelectrode Array. *Nanotechnology* **2008**, *19*, 275301.
(43) Han, S.; Briseno, A. L.; Shi, X.; Mah, D. A.; Zhou, F. Polyelectrolyte-Coated Nanosphere Lithographic Patterning of Surfaces: Fabrication and Characterization of Electropolymerized Thin Polyaniline Honeycomb Films. *J. Phys. Chem. B* **2002**, *106*, 6465−6472.
(44) Kazimierska, E.; Smyth, M. R.; Killard, A. J. Size-Dependent Electrocatalytic Reduction of Nitrite at Nanostructured Films of Hollow Polyaniline Spheres and Polyaniline−Polystyrene Core−Shells. *Electrochim. Acta* **2009**, *54*, 7260−7267.
(45) Cernat, A.; Le Goff, A.; Holzinger, M.; Sandulescu, R.; Cosnier, S. Micro- to Nanostructured Poly(Pyrrole-Nitrilotriacetic Acid) Films via Nanosphere Templates: Applications to 3D Enzyme Attachment by Affinity Interactions. *Anal. Bioanal. Chem.* **2014**, *406*, 1141−1147.
(46) Yang, X.; Jin, Y.; Zhu, Y.; Tang, L.; Li, C. Inverse Opal of Polyaniline for Biosensors Prepared by Electrochemical and Self-Assembly Techniques. *J. Electrochem. Soc.* **2008**, *155*, J23−J25.
(47) Norris, D. J.; Vlasov, Y. A. Chemical Approaches to Three-Dimensional Semiconductor Photonic Crystals. *Adv. Mater.* **2001**, *13*, 371−376.
(48) Shkunov, M. N.; Vardeny, Z. V.; DeLong, M. C.; Polson, R. C.; Zakhidov, A. A.; Baughman, R. H. Tunable, Gap-State Lasing in Switchable Directions for Opal Photonic Crystals. *Adv. Funct. Mater.* **2002**, *12*, 21−26.
(49) Schwartz, B. J.; Nguyen, T.-Q.; Wu, J.; Tolbert, S. H. Interchain and Intrachain Exciton Transport in Conjugated Polymers: Ultrafast Studies of Energy Migration in Aligned MEH-PPV/Mesoporous Silica Composites. *Synth. Met.* **2001**, *116*, 35−40.
(50) Fritea, L.; Haddache, F.; Reuillard, B.; Le Goff, A.; Gorgy, K.; Gondran, C.; Holzinger, M.; Săndulescu, R.; Cosnier, S. Electrochemical Nanopatterning of an Electrogenerated Photosensitive Poly-[Trisbipyridinyl-Pyrrole Ruthenium(II)] Metallopolymer by Nanosphere Lithography. *Electrochem. Commun.* **2014**, *46*, 75−78.
(51) Xu, L.; Wang, J.; Song, Y.; Jiang, L. Electrically Tunable Polypyrrole Inverse Opals with Switchable Stopband, Conductivity, and Wettability. *Chem. Mater.* **2008**, *20*, 3554−3556.
(52) Santos, L.; Martin, P.; Ghilane, J.; Lacaze, P. C.; Lacroix, J.-C. Micro/Nano-Structured Polypyrrole Surfaces on Oxidizable Metals as Smart Electroswitchable Coatings. *ACS Appl. Mater. Interfaces* **2013**, *5*, 10159−10164.
(53) Sakmeche, N.; Aeiyach, S.; Aaron, J.-J.; Jouini, M.; Lacroix, J. C.; Lacaze, P.-C. Improvement of the Electrosynthesis and Physicochemical Properties of Poly(3,4-Ethylenedioxythiophene) Using a Sodium Dodecyl Sulfate Micellar Aqueous Medium. *Langmuir* **1999**, *15*, 2566−2574.
(54) Han, M. G.; Foulger, S. H. Facile Synthesis of Poly(3,4-ethylenedioxythiophene) Nanofibers from an Aqueous Surfactant Solution. *Small* **2006**, *2*, 1164−1169.
(55) Du, X.-S.; Zhou, C.-F.; Mai, Y.-W. Novel Synthesis of Poly(3,4-Ethylenedioxythiophene) Nanotubes and Hollow Micro-Spheres. *Mater. Lett.* **2009**, *63*, 1590−1593.
(56) Duvail, J. L.; Long, Y.; Cuenot, S. p.; Chen, Z.; Gu, C. Tuning Electrical Properties of Conjugated Polymer Nanowires with the Diameter. *Appl. Phys. Lett.* **2007**, *90*, 102114.
(57) Duvail, J. L.; Rétho, P.; Fernandez, V.; Louarn, G.; Molinié, P.; Chauvet, O. Effects of the Confined Synthesis on Conjugated Polymer Transport Properties. *J. Phys. Chem. B* **2004**, *108*, 18552−18556.
(58) Baba, A.; Lübben, J.; Tamada, K.; Knoll, W. Optical Properties of Ultrathin Poly(3,4-ethylenedioxythiophene) Films at Several Doping Levels Studied by In Situ Electrochemical Surface Plasmon Resonance Spectroscopy. *Langmuir* **2003**, *19*, 9058−9064.
(59) Kaune, G.; Memesa, M.; Meier, R.; Ruderer, M. A.; Diethert, A.; Roth, S. V.; D'Acunzi, M.; Gutmann, J. S.; Müller-Buschbaum, P. Hierarchically Structured Titania Films Prepared by Polymer/Colloidal Templating. *ACS Appl. Mater. Interfaces* **2009**, *1*, 2862−2869.
(60) Kei, C.-C.; Kuo, K.-H.; Su, C.-Y.; Lee, C.-T.; Hsiao, C.-N.; Perng, T.-P. Metal Oxide Nano-Honeycombs Prepared by Solution-Based Nanosphere Lithography and the Field Emmission Properties. *Chem. Mater.* **2006**, *18*, 4544−4546.
(61) Sun, F.; Cai, W.; Li, Y.; Cao, B.; Lei, Y.; Zhang, L. Morphology-Controlled Growth of Large-Area Two-Dimensional Ordered Pore Arrays. *Adv. Funct. Mater.* **2004**, *14*, 283−288.
(62) Cassie, A.; Baxter, S. Wettability of Porous Surfaces. *Trans. Faraday Soc.* **1944**, *40*, 546−551.
(63) Choi, H.-J.; Choo, S.; Shin, J.-H.; Kim, K.-I.; Lee, H. Fabrication od Superhydrophobic and Oleophobic Surfaces with Overhang Structure by Reverse Nanoimprint Lithography. *J. Phys. Chem. C* **2013**, *117*, 24354−24359.
(64) Abdelsalam, M. E.; Bartlett, P. N.; Kelf, T.; Baumberg, J. Wetting of Regularly Structured Gold Surfaces. *Langmuir* **2005**, *21*, 1753−1757.
(65) Zhu, Y.; Hu, D.; Wan, M.; Jiang, L.; Wei, Y. Conducting and Superhydrophobic Rambutan-Like Hollow Spheres of Polyaniline. *Adv. Mater.* **2007**, *19*, 2092−2096.
(66) O'Regan, B.; Gratzel, M. A Low-Cost, High-Efficiency Solar Cell Based on Dye-Sensitized Colloidal TiO_2 Films. *Nature* **1991**, *353*, 737−740.

DOI: 10.1021/acsami.5b06699
ACS Appl. Mater. Interfaces 2015, 7, 21673−21681

(67) Saito, Y.; Kitamura, T.; Wada, Y.; Yanagida, S. Application of Poly(3,4-ethylenedioxythiophene) to Counter Electrode in Dye-Sensitized Solar Cells. *Chem. Lett.* **2002**, *31*, 1060−1061.
(68) Biallozor, S.; Kupniewska, A. Study on Poly(3,4-Ethylenedioxythiophene) Behaviour in the I^-/I_2 Solution. *Electrochem. Commun.* **2000**, *2*, 480−486.
(69) Cho, B.; Park, K. S.; Baek, J.; Oh, H. S.; Koo Lee, Y.-E.; Sung, M. M. Single-Crystal Poly(3,4-ethylenedioxythiophene) Nanowires with Ultrahigh Conductivity. *Nano Lett.* **2014**, *14*, 3321−3327.
(70) Balis, N.; Makris, T.; Dracopoulos, V.; Stergiopoulos, T.; Lianos, P. Quasi-Solid-State Dye-Sensitized Solar Cells Made with Poly(3,4-Ethylenedioxythiophene)-Functionalized Counter-Electrodes. *J. Power Sources* **2012**, *203*, 302−307.

DOI: 10.1021/acsami.5b06699
ACS Appl. Mater. Interfaces 2015, 7, 21673−21681